Nanoparticle Properties

DOI: 10.1002/anie.200906130

Synthetic Tuning of the Catalytic Properties of Au-Fe_3O_4 Nanoparticles**

*Youngmin Lee, Miguel Angel Garcia, Natalie A. Frey Huls, and Shouheng Sun**

Metal nanoparticles (NPs), and in particular Au NPs, dispersed on an oxide support often show a much higher catalytic activity than the single-component NPs.[1–6] Such catalytic enhancement is attributed to the synergetic effect that occurs at the interface of metal and oxide support.[1–3,5,7–11] It is believed that the electronic structures of both the metal and the oxide support are modified by electron transfer across the interface, giving rise to oxygen vacancies on the interfacial oxide support that become active sites for oxygen absorption and activation.[7,10–12] Recent studies seem to indicate that small Au clusters in the junction structure are the real active source for catalysis.[5,13] These small Au clusters have more low-coordinate Au atoms than extended Au crystal surfaces, and have higher energy *d* states, which are more reactive and absorb/activate O_2 molecules more readily. This hypothesis is further supported by a very recent microscopy study on an Au/FeO_x catalyst system, in which the origin of the Au activity on CO oxidation is associated uniquely with Au bilayer clusters that are circa 0.5 nm in diameter and contain about 10 Au atoms.[13] Despite these efforts in understanding the synergetic effect in catalyst/support systems and the general belief that catalyst/support interface boundary sites are important for the enhanced catalysis, there is very limited study on monodisperse catalyst/support with both catalyst and support in nanometer scale,[14] and there is no direct evidence that the synergetic effect is present in the composite catalyst.

Herein we show that the dumbbell-like Au-Fe_3O_4 NPs indeed show a synergetic effect in catalyzing H_2O_2 reduction. Dumbbell-like Au-Fe_3O_4 NPs were synthesized, and single-component Au and Fe_3O_4 NPs were formed from Au-Fe_3O_4 NPs by a controlled etching of Au-Fe_3O_4 NPs, which ensures that the individual Au and Fe_3O_4 NPs have the same structural features as the Au-Fe_3O_4 NPs. We demonstrate that the dumbbell-like Au-Fe_3O_4 NPs are catalytically more active than either Au or Fe_3O_4 NPs for H_2O_2 reduction.

[*] Y. Lee, Dr. N. A. Frey Huls, Prof. S. Sun
Department of Chemistry, Brown University
Providence, RI 02912 (USA)
Fax: (+1) 401-863-9046
E-mail: ssun@brown.edu
Dr. M. A. Garcia
Instituto de Ceramica y Vidrio, CSIC, C/Kelsen 5
Campus de Cantoblanco, 28049 Madrid (Spain)

[**] This work was supported by NSF/DMR 0606264 (S.S.), a GAANN fellowship (Y.L.), and CICYT/FIS-2008-06249 (M.A.G.). We thank Prof. H. Srikanth and Dr. M. H. Phan of the University of South Florida for helpful discussions.

Supporting information for this article is available on the WWW under http://dx.doi.org/10.1002/anie.200906130.

The dumbbell-like Au-Fe_3O_4 NPs were synthesized by controlled nucleation of Fe_3O_4 on Au NPs (see the Experimental Section). The Au seeding NPs were made by the reduction of $HAuCl_4 \cdot 3H_2O$ by *tert*-butylamine–borane (TBAB) in 1,2,3,4-tetrahydronaphthalene (tetralin) and oleylamine.[15] The Au NP sizes were controlled by the temperature at which TBAB was injected. To synthesize Au-Fe_3O_4 NPs, $[Fe(CO)_5]$ was injected into a 1-octadecene solution containing these Au seeds. Iron then nucleated and grew on the Au NPs. Upon exposure to air, the Fe NPs were oxidized to Fe_3O_4 NPs, giving Au-Fe_3O_4 NPs.[16,17] Figure 1 a,b shows transmission electron microscopy (TEM) images of 6 nm Au seeding NPs and 6–17 nm Fe_3O_4 NPs. 3–17 nm Au-Fe_3O_4 NPs and 8–20 nm Au-Fe_3O_4 NPs (Supporting Information, Figure S1 a,b) were also prepared so that the size-dependent catalytic properties of Au-Fe_3O_4 could be compared.

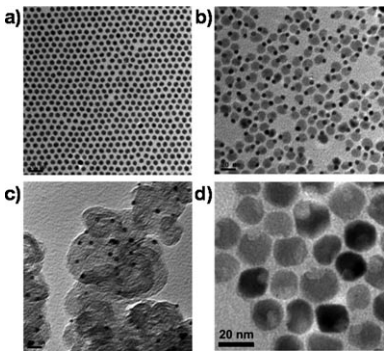

Figure 1. TEM images of the as-synthesized a) 6 nm Au NPs, b) 6–17 nm Au-Fe_3O_4 NPs obtained by using (a) as Au seeds, c) the 6 nm Au NPs on carbon obtained by etching Fe_3O_4 away from (b), and d) dented 17 nm Fe_3O_4 NPs obtained by etching Au away from the Au-Fe_3O_4 NPs. Scale bars: 20 nm.

The single-component Au NP catalyst was obtained by etching Fe_3O_4 away from the Au-Fe_3O_4 NPs on carbon catalyst in 0.5 M H_2SO_4 (Scheme 1).[17] This reaction takes advantage of the stability difference between Au and Fe_3O_4 in acid solution: Fe_3O_4 can be dissolved while Au stays intact. To prevent Au NPs from aggregation after acid etching of Fe_3O_4, Au-Fe_3O_4 NPs were first deposited on the Ketjen carbon

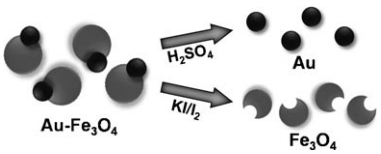

Scheme 1. Selected etching of Au-Fe_3O_4 NPs for the preparation of the Au NPs and dented Fe_3O_4 NPs.

support. (The same support was also used for H_2O_2 reduction studies by ultrasonification of the Au-Fe_3O_4 NPs and carbon in hexane for two hours followed by hexane evaporation.) The TEM image shows that the Au-Fe_3O_4 NPs are well-dispersed on the carbon support (Supporting Information, Figure S2). The dried Au-Fe_3O_4/C was immersed in 0.5 M H_2SO_4 for 3 h to obtained Au/C. The single-component Fe_3O_4 NP catalyst was obtained by a two-phase etching of Au from Au-Fe_3O_4 NPs using KI/I_2 solution (Scheme 1).[18] KI is used to improve the solubility of AuI formed by $2\,Au + I_2 \rightarrow 2\,AuI$. This two-phase system is useful for facile separation and re-dispersion of the Fe_3O_4 NPs after the selective Au etching. We also attempted to separate Au and Fe_3O_4 from Au-Fe_3O_4 NPs by directly heating the NP dispersion in 1-octadecene at 180 °C. However, the majority of the dumbbell structure stayed intact, apart from continued Ostwald ripening seen as some of the Au NPs grew larger and others became smaller (Supporting Information, Figure S3). After three hours of the thermal treatment, most of the Au-Fe_3O_4 NPs aggregated.

Figure 1 c,d shows the TEM images of the 6 nm Au/C after etching Fe_3O_4 from the Au-Fe_3O_4/C, and the 17 nm Fe_3O_4 NPs obtained from the Au-Fe_3O_4 NPs after Au etching. Compared with the Au-Fe_3O_4 NPs in Figure 1 b, both the Au NPs and the Fe_3O_4 NPs show no obvious size change during the etching processes, except that the Fe_3O_4 NPs obtained from the Au etching have dents, which confirm that the Fe_3O_4 NPs indeed form the side-by-side junctions with the Au NPs in the dumbbell-like Au-Fe_3O_4 structure. Figure 2 shows a series of X-ray diffraction (XRD) patterns of the Au-Fe_3O_4 and the Au and Fe_3O_4 NPs obtained from the etching of Au-Fe_3O_4 NPs. The peaks from the Au and Fe_3O_4 NPs match well with those in Au-Fe_3O_4 NPs: there is no peak shift or peak width change, thus further indicating that crystal structures of Au and Fe_3O_4 NPs are also preserved during the etching processes.

The etching experiments offer two single-component NPs of Au and Fe_3O_4 that are directly from the Au-Fe_3O_4. The synergetic effect can be better illustrated by comparing catalytic properties of the Au-Fe_3O_4 NPs with Au NPs and/or Fe_3O_4 NPs. In these comparative catalytic studies, we did not select Au seeding NPs and Fe_3O_4 NPs prepared from the reductive decomposition of [Fe(acac)$_3$] or thermal decomposition of [$Fe(CO)_5$] followed by oxidation,[19–21] as the structure/morphology of these individual NPs are different from those in Au-Fe_3O_4 NPs.

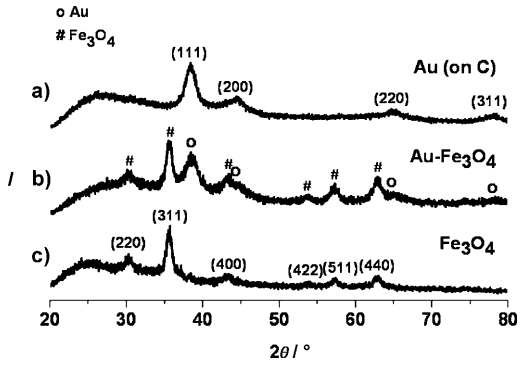

Figure 2. XRD patterns of a) Au NPs obtained by etching Fe_3O_4 away from Au-Fe_3O_4, b) Au-Fe_3O_4 NPs (○ Au, # Fe_3O_4), and c) dented Fe_3O_4 NPs obtained by etching Au away from Au-Fe_3O_4 NPs.

We chose the reduction of H_2O_2 to H_2O in neutral phosphate-buffered saline (PBS) solution as a model reaction to demonstrate that the synergetic effect present in the Au-Fe_3O_4 structure does offer the enhanced catalysis for the reduction reaction. Such a reaction catalyzed by NP catalysts has been explored extensively to develop electrochemical sensor for H_2O_2 detection[22–38] and for biomedical applications.[39,40] The synthetic tuning of the NP catalyst to its maximum activity is a key step in optimizing the device to detect H_2O_2 at ultralow concentrations.

The as-synthesized Au-Fe_3O_4 NPs were washed with ethanol to remove as much oleylamine surfactant as possible, dried under N_2 and re-dispersed in hexane. The NP hexane dispersion (10 mg NPs/10 mL hexane) was mixed with the Ketjen carbon (30 mg) and ultrasonicated for 2 hours. The NP/C composite was washed with hexane to remove the loosely bound NPs and dried under N_2 to give 25 wt % of Au-Fe_3O_4 NPs on carbon. The composite catalyst was then suspended in water at a concentration of 2 mg mL^{-1} and sonicated for one hour for electrocatalytic studies.

Catalysis of H_2O_2 reduction was studied by cyclic voltammetry (see the Experimental Section). Figure 3 a,b shows the *I–V* curves reflecting H_2O_2 reduction catalyzed by Au-Fe_3O_4, Au, and Fe_3O_4 NPs in 0.1 M PBS/4 mM H_2O_2 solution. Comparing the *I–V* curves from Au and Au-Fe_3O_4 NPs (Figure 3 a), we can see that the Au-Fe_3O_4 NPs are more active for H_2O_2 reduction; they have more positive onset potential and larger reduction current than the Au NPs. H_2O_2 reduction occurs fairly readily on both Au-Fe_3O_4 and the dented Fe_3O_4 NPs (Figure 3 b), with the two catalysts showing similar onset potentials, but the Au-Fe_3O_4 NPs generate much higher reduction current at the same applied potential. No activity was observed on just carbon support (Figure 3 c) or

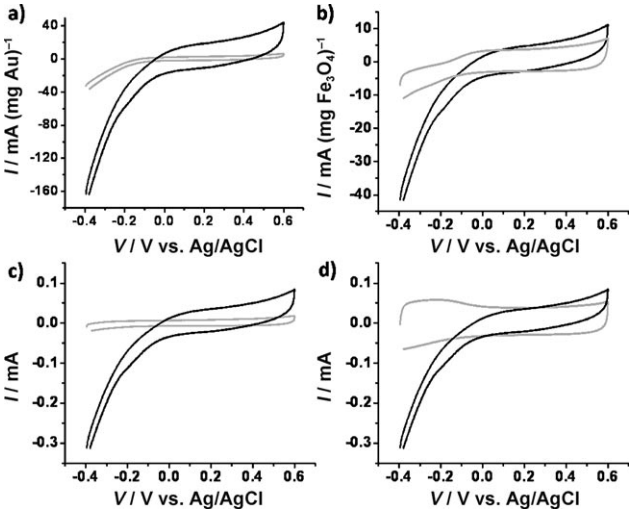

Figure 3. *I–V* curves of a) Au-Fe_3O_4 (black) and Au NP (gray), b) Au-Fe_3O_4 (black) and Fe_3O_4 NP catalysts (gray) normalized by Au and Fe_3O_4 weight, respectively, c) Au-Fe_3O_4 catalyst (black) and carbon support (gray), and d) Au-Fe_3O_4 catalyst with (black) and without (gray) the addition of 4 mM of H_2O_2. Recorded in N_2-saturated 0.1 M PBS with 4 mM of H_2O_2; rotation speed: 1600 rpm, scan rate: 50 mV s^{-1}.

from the Au-Fe_3O_4/C catalyst in the absence of H_2O_2 (Figure 3d), thus indicating that the catalytic activity arises from the NP catalyst.

Au-Fe_3O_4/C catalysts with different sizes of Au NPs (8 nm, 3 nm) were also studied for the catalytic H_2O_2 reduction in the presence of 4 mM of H_2O_2. (*I–V* curves of 8–20 nm Au-Fe_3O_4 NPs and 3–17 nm Au-Fe_3O_4 NPs are given in the Supporting Information, Figure S4.) Au-Fe_3O_4 NPs with 8 nm Au show higher activity and stability after 100 cycles of reduction than those with 3 nm Au. Combining these results together with what we observed from 6–17 nm Au-Fe_3O_4 NPs, we can conclude that the Au-Fe_3O_4 NPs indeed show the enhanced catalysis for H_2O_2 reduction, and the larger Au NPs offer even higher activity due to the larger interconnection area between Au and Fe_3O_4.

Previous research has shown that Au NPs deposited on various oxide supports, including iron oxide supports, are catalytically more active for oxidation reaction due to the Au NP polarization towards the support at the interface.[1,3,5] However, our recent study finds that Au NPs in Au-Fe_3O_4 NPs are less active for oxygen reduction reaction in alkaline solution.[17] These studies indicate that there is an interaction between Au and Fe_3O_4, but Au NPs in the Au-Fe_3O_4 structure should not show the enhanced catalysis for the H_2O_2 reduction reaction. The enhanced catalysis observed in Au-Fe_3O_4 NPs must come from the Fe_3O_4, for which the polarization at the interface makes the Fe_3O_4 NP more active for H_2O_2 reduction. This observation was further confirmed by the control experiments: the mixture of Au and Fe_3O_4 NPs[41] exhibited much less activity than the Au-Fe_3O_4 NPs in the reduction catalysis (Supporting Information, Figure S5); the solution after Fe_3O_4 NP removal did not show any catalytic activity in the current detection conditions. Therefore, the reduction activity does not arise from the free Fe ions that can catalyze the H_2O_2 decomposition, as in Fenton's reaction,[42] but rather comes from the surface of the Fe_3O_4 NPs;[43] this activity is further enhanced by their epitaxial link with Au NPs.

Studies on the optical properties of the Au-Fe_3O_4 NPs further support a strong interfacial interaction between Au and Fe_3O_4 in Au-Fe_3O_4 NPs. From the surface plasmon resonance (SPR) absorption spectra of the Au-Fe_3O_4 NPs, we observed a red shift of the absorption peak compared to that of the Au seeds.[16] Our further modeling studies indicate the absorption peak of the Au-Fe_3O_4 NPs fits well with the calculated absorption value of 2.8 nm Au NPs rather than that of the 6.26 nm (the average size of Au in Au-Fe_3O_4 NPs measured from TEM images, Figure 4). The electron configuration of the Au NPs is thus modified by the interconnected Fe_3O_4, restraining part of the electrons of Au and resulting in a damping of the collective oscillation.

In summary, we have developed a unique synthesis of Au, Fe_3O_4, and Au-Fe_3O_4 NPs. Different from all previous synthesis, the single-component Au and Fe_3O_4 NPs are obtained directly from the Au-Fe_3O_4 NPs by either Au etching or Fe_3O_4 etching, which allows the direct comparison of NP catalysis for H_2O_2 reduction and shows that the Au-Fe_3O_4 NPs offer the enhanced catalysis. By studying the H_2O_2 reduction catalyzed by the individual Au and Fe_3O_4 NPs, we can demonstrate experimentally that the enhanced catalysis of Au-Fe_3O_4 arises from the polarization effect at the Au-Fe_3O_4 interface, where Fe_3O_4 becomes more active. As the sizes of both Au and Fe_3O_4 in the Au-Fe_3O_4 structure can be tuned synthetically, the Au-Fe_3O_4 NPs offer an ideal catalyst system for studying synergetic effects that are controlled not only by Au but also by Fe_3O_4. This nanostructure tuning capability should also allow the development of active Au-Fe_3O_4 NPs for highly sensitive H_2O_2 detection.

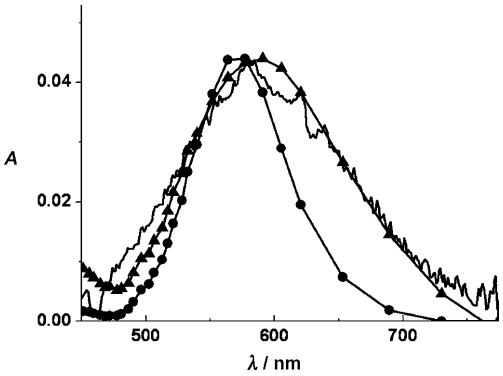

Figure 4. Absorption spectrum of the Au-Fe_3O_4 NPs, the calculated absorbance value for 6 nm Au in the Au-Fe_3O_4 NPs structure (●), and the calculated absorbance for Au that shows closer value to the Au-Fe_3O_4 NPs (▲). For both experimental and calculated spectra, a linear background was subtracted in order to account for other contributions to the absorption spectrum.

Experimental Section

$HAuCl_4 \cdot 3H_2O$ (Strem Chemicals), *tert*-butylamine–borane (TBAB, 97%, Sigma–Aldrich), oleylamine (80–90%, Acros Organics), oleic acid (80–90%, Acros Organics), 1,2,3,4-tetrahydronaphthalene (tetralin, 99%, Sigma–Aldrich), 1-octadecene (90%, Sigma–Aldrich), Nafion 117 (ca. 5%, Fluka), $[Fe(CO)_5]$ (98%, Sigma–Aldrich), 0.1M phosphate-buffered saline (PBS; without Ca, Mg; MP Biomedicals, LLC), sulfuric acid (Mallinckrodt), potassium iodide (Sigma-Aldirch), iodine (Sigma-Aldirch), and hydrogen peroxide (50 wt% in water, Sigma–Aldrich) were used as received.

Au NPs: For a typical synthesis of 6 nm Au NPs, a solution of tetralin (10 mL), oleylamine (10 mL), and $HAuCl_4 \cdot 3H_2O$ (0.1 g) was prepared at room temperature (20°C) and initially stirred for 10 min. TBAB (1 mmol), tetralin (1 mL), and oleylamine (1 mL) were mixed by sonication and quickly injected into the above solution. The reaction mixture was further stirred at room temperature for 1 h. Au NPs were precipitated by ethanol addition and collected by centrifugation. The product was re-dispersed in hexane and separated by ethanol addition and centrifugation. This procedure was repeated three times. The final product, 6 nm Au NPs, was dispersed in hexane. Different sizes of Au NPs were obtained by controlling the temperatures at which the TBAB was injected.

Au-Fe_3O_4 NPs: Pre-synthesized 6 nm Au NP seeds (20 mg) in hexane (1 mL) were added to a solution of 20 mL of 1-octadecene with oleic acid (1 mL) and oleylamine (1 mL). The mixture was heated up to 120°C under a gentle N_2 flow to remove hexane. Under a N_2 blanket, $[Fe(CO)_5]$ (0.1 mL) was injected into the solution. The solution was heated to reflux (300°C) and left at that temperature for 30 min. Thereafter, it was cooled down to room temperature and was exposed to air to form Au-Fe_3O_4 NPs. Isopropanol was added to precipitate the Au-Fe_3O_4 NPs, which were collected by centrifugation. The product was re-dispersed in hexane and separated by adding

ethanol and centrifugation. This procedure was repeated three times. The 6–17 nm Au-Fe_3O_4 NPs were then dispersed in hexane.

Etching Fe_3O_4 away from Au-Fe_3O_4 NPs: 50 wt% of the Au-Fe_3O_4 NPs on carbon support (40 mg total) were mixed in hexane then dried with nitrogen. The carbon support was needed to prevent aggregation of Au during etching. H_2SO_4 (0.5 M, 10 mL) was added to the mixture, and the mixture was sonicated for 3 h. The catalysts were separated and washed with deionized water three times. The final product was separated by centrifugation.

Etching Au away from Au-Fe_3O_4 NPs: Two-phase etching was carried out to remove Au from Au-Fe_3O_4 NPs. KI (800 mg) and iodine (200 mg) were mixed in deionized water (10 mL). The KI/I_2 solution (10 mL) was added to a vial containing Au-Fe_3O_4 NPs (ca. 30 mg) in a hexane dispersion. The mixture was shaken for one hour, and the hexane phase was collected in a centrifuge tube. The etched Fe_3O_4 NPs were separated by adding ethanol and centrifugation.

Electrochemical measurements: NPs were dried under N_2 and deposited on carbon support (Ketjen carbon, surface area 800 $m^2 g$) by ultrasonification for 2 h in hexane (25 wt% of NPs on carbon). The dried catalyst (NP/C) was then prepared in water (2 mg mL^{-1}) and was sonicated for 1 h. 20 μL of the mixture was added to the glassy carbon rotating-disk working electrode (5 mm in diameter, mirror-polished), and water was dried in vacuum. Afterwards, the catalyst was covered with a thin layer of Nafion (0.1% in water, 10 μL) to ensure that the NP catalyst was tightly attached to the electrode surface during the electrochemical measurements. The precise weight percentage of Au in Au-Fe_3O_4 NPs was obtained by dissolving Au-Fe_3O_4 NPs in aqua regia and measuring the Au concentration with inductively coupled plasma atomic-emission spectroscopy (ICP-AES). Cyclic voltammetry measurements were performed on a Pine Electrochemical Analyzer, Model AFCBP1. Ag/AgCl and Pt wire were used as reference and counter electrodes, respectively. The reaction was carried out in 0.1 M PBS solution (pH 7.4) at room temperature (22 °C). The catalyst was cleaned to remove the surfactant residue by pre-scanning in the test solution between −400 mV and 600 mV for 20 cycles under a saturated N_2 atmosphere. H_2O_2 reduction was monitored at the rotation speed of 1600 rpm (rotations per minute) under N_2 saturation conditions.

Optical absorption measurements were performed at room temperature with a Shimadzu 3100 double-beam spectrophotometer attached with an integrating sphere in the transmission mode. Samples were deposited onto a glass substrate and placed in the beam path. The beam spot was 4 × 4 mm at the sample surface. Calculated spectra were obtained following the Mie theory for spherical nanoparticles using a dielectric function corrected for small-size effects. For both experimental and calculated spectra, a linear background was subtracted to account for other contributions to the absorption spectrum.

Samples for transmission electron microscopy (TEM) analysis were prepared by depositing and drying a single drop of diluted Au NP dispersion in hexane on amorphous-carbon-coated copper grids under ambient conditions. Images were obtained by a Philips EM 420 (120 kV). Powder X-ray diffraction (XRD) patterns were obtained on a Bruker AXS D8-Advanced diffractometer with $Cu_{K\alpha}$ radiation ($\lambda = 1.5418$ Å).

Received: October 30, 2009
Published online: January 13, 2010

Keywords: electrochemistry · gold · heterogeneous catalysis · hydrogen peroxide reduction · nanoparticles

[1] M. Haruta, N. Yamada, T. Kobayashi, S. Iijima, *J. Catal.* **1989**, *115*, 301.
[2] M. Haruta, *Catal. Today* **1997**, *36*, 153.
[3] M. Haruta, *CATTECH* **2002**, *6*, 102.
[4] M. Valden, X. Lai, D. W. Goodman, *Science* **1998**, *281*, 1647.
[5] M. S. Chen, D. W. Goodman, *Science* **2004**, *306*, 252.
[6] C. Milone, R. Ingoglia, S. Galvagno, *Gold Bull.* **2006**, *39*, 54.
[7] Z.-P. Liu, X.-Q. Gong, J. Kohanoff, C. Sanchez, P. Hu, *Phys. Rev. Lett.* **2003**, *91*, 266102.
[8] N. F. Zheng, G. D. Stucky, *J. Am. Chem. Soc.* **2006**, *128*, 14278.
[9] M. Comotti, W. C. Li, B. Spliethoff, F. Schuth, *J. Am. Chem. Soc.* **2006**, *128*, 917.
[10] J. D. Grunwaldt, A. Baiker, *J. Phys. Chem. B* **1999**, *103*, 1002.
[11] L. M. Molina, B. Hammer, *Phys. Rev. Lett.* **2003**, *90*, 206102-1.
[12] M. M. Schubert, S. Hackenberg, A. C. van Veen, M. Muhler, V. Plzak, R. J. Behm, *J. Catal.* **2001**, *197*, 113.
[13] A. A. Herzing, C. J. Kiely, A. F. Carley, P. Landon, G. J. Hutchings, *Science* **2008**, *321*, 1331.
[14] H. F. Yin, C. Wang, H. G. Zhu, S. H. Overbury, S. H. Sun, S. Dai, *Chem. Commun.* **2008**, 4357.
[15] S. Peng, Y. Lee, C. Wang, H. Yin, S. Dai, S. Sun, *Nano Res.* **2008**, *1*, 229.
[16] H. Yu, M. Chen, P. M. Rice, S. X. Wang, R. L. White, S. H. Sun, *Nano Lett.* **2005**, *5*, 379.
[17] Y. Lee, A. Loew, S. Sun, *Chem. Mater.* **2009**, DOI: 10.1021/cm9013046.
[18] W. F. Gale, T. C. Totemeier, *Smithells Metals Reference Book*, Eighth Edition, Elsevier Butterworth Heinemann, Oxford, **2004**.
[19] S. Sun, H. Zeng, *J. Am. Chem. Soc.* **2002**, *124*, 8204.
[20] T. Hyeon, S. S. Lee, J. Park, Y. Chung, H. B. Na, *J. Am. Chem. Soc.* **2001**, *123*, 12798.
[21] Z. Xu, C. Shen, Y. Hou, H. Gao, S. Sun, *Chem. Mater.* **2009**, *21*, 1778.
[22] O. S. Wolfbeis, A. Dürkop, M. Wu, Z. Lin, *Angew. Chem.* **2002**, *114*, 4681; *Angew. Chem. Int. Ed.* **2002**, *41*, 4495.
[23] D. X. Cao, J. D. Chao, L. M. Sun, G. L. Wang, *J. Power Sources* **2008**, *179*, 87.
[24] A. Barbouti, P.-T. Doulias, B.-Z. Zhu, B. Frei, D. Galaris, *Free Radical Biol. Med.* **2001**, *31*, 490.
[25] D. A. Stavreva, T. Gichner, *Mutat. Res. Genet. Toxicol. Environ. Mutagen.* **2002**, *514*, 147.
[26] X. Yi, J. Huang-Xian, C. Hong-Yuan, *Anal. Biochem.* **2000**, *278*, 22.
[27] J. Jia, B. Wang, A. Wu, G. Cheng, Z. Li, S. Dong, *Anal. Chem.* **2002**, *74*, 2217.
[28] J.-J. Feng, G. Zhao, J.-J. Xu, H.-Y. Chen, *Anal. Biochem.* **2005**, *342*, 280.
[29] J. Zhang, M. Oyama, *J. Electroanal. Chem.* **2005**, *577*, 273.
[30] J. Di, C. Shen, S. Peng, Y. Tu, S. Li, *Anal. Chim. Acta* **2005**, *553*, 196.
[31] Y. H. Lu, M. H. Yang, F. L. Qu, G. L. Shen, R. Q. Yu, *Bioelectrochemistry* **2007**, *71*, 211.
[32] S. Guo, E. Wang, *Anal. Chim. Acta* **2007**, *598*, 181.
[33] J. Hong, Z. Dai, *Sens. Actuators B* **2009**, *140*, 222.
[34] A. M. Yu, Z. J. Liang, J. H. Cho, F. Caruso, *Nano Lett.* **2003**, *3*, 1203.
[35] B. I. Ipe, K. Yoosaf, K. G. Thomas, *J. Am. Chem. Soc.* **2006**, *128*, 1907.
[36] N. Zhou, J. Wang, T. Chen, Z. Yu, G. Li, *Anal. Chem.* **2006**, *78*, 5227.
[37] Y. Xiao, F. Patolsky, E. Katz, J. F. Hainfeld, I. Willner, *Science* **2003**, *299*, 1877.
[38] S. Guo, D. Wen, S. Dong, E. Wang, *Talanta* **2009**, *77*, 1510.
[39] T. P. Szatrowski, C. F. Nathan, *Cancer Res.* **1991**, *51*, 794.
[40] M. Lopez-Lazaro, *Cancer Lett.* **2007**, *252*, 1.
[41] These particles were synthesized according to the procedures reported in references [15] and [21].
[42] C. L. Hsueh, Y. H. Huang, C. C. Wang, C. Y. Chen, *Chemosphere* **2005**, *58*, 1409.
[43] L. Gao, J. Zhuang, L. Nie, J. Zhang, Y. Zhang, N. Gu, T. Wang, J. Feng, D. Yang, S. Perrett, X. Yan, *Nat. Nanotechnol.* **2007**, *2*, 577.

